Journal of Materials Chemistry C

Full paper

Tungstate nanosheet ink as a photonless and electroless chromic device

Masahiro Miyauchi,[*ab] **Akihiko Kondo,**[a] **Daiki Atarashi**[a] **and Etsuo Sakai**[a]

5 Cesium tungstate ($Cs_4W_{11}O_{36}{}^{2-}$) nanosheets coated on an aluminum (Al) substrate turned blue in an aqueous solution, which acts as an ink, and rapidly decolorized under air exposure, which acts an eraser. The decoloration rate of $Cs_4W_{11}O_{36}{}^{2-}$ nanosheets was several orders of magnitude more efficient than that of conventional tungsten trioxide (WO_3) particles, owing to efficient electron transfer in nanosheet structure.

10 1 Introduction

Chromism is a process that causes a reversible color change in materials in response to an external stimulus and is useful for various industrial applications, such as displays, sensors, and data storage. Photochromism and electrochromism are transformations 15 that are induced by stimulations with light irradiation and an electric field, respectively.[1-4] Among chromic materials, tungsten trioxide (WO_3) exhibits efficient photochromic and electrochromic properties reactivity.[5-8] However, during the coloration of WO_3 under light irradiation, electrons are trapped at 20 deep levels, and the rate of the decoloration process is very slow in air.[9] As an electrochromic material, WO_3 requires complicated apparatus and electrode structure, including an electric power supply and a complicated sandwich-type cell with a transparent electroconductive substrate, such as indium–tin-oxide (ITO), and 25 a counter electrode filled with an electrolyte solution.[2, 4]

Recently, we reported that a WO_3-based chromic device is capable of functioning without light irradiation or an electric power supply.[10] The WO_3-coated aluminum (Al) substrate turns a dark color upon exposure to an aqueous solution, with subsequent 30 exposure to oxygen restoring the original light-yellow color of the material. Although this phenomenon is similar to solvatochromism in organic chromophore molecules,[11] the color change in WO_3/Al is due to the galvanic potential between WO_3 and Al, rather than as a result of the polarity of solvent. This WO_3 35 based chromic device exhibits high stability against thermal or chemical treatment rather than a solvatochromic device using organic chromophore molecules. Herein, we developed an efficient galvanic chromic device composed of a film of layered cesium tungstate ($Cs_4W_{11}O_{36}{}^{2-}$) nanosheets, which are transparent 40 in the visible-light range due to the quantum confinement effect. $Cs_4W_{11}O_{36}{}^{2-}$ nanosheets coated on an aluminum (Al) substrate exhibited a rapid, reversible color change. $Cs_4W_{11}O_{36}{}^{2-}$/Al turned blue in an aqueous acid solution, and rapidly decolorized under air exposure. In this device, the aqueous solvent acts as an ink, 45 while oxygen exposure acts as an eraser. The color change was due to the galvanic potential between $Cs_4W_{11}O_{36}{}^{2-}$ and Al, and the decoloration rate of $Cs_4W_{11}O_{36}{}^{2}$ is 25-fold higher than that of WO_3 particles. The efficient color change is due to the nanostructure of the $Cs_4W_{11}O_{36}{}^{2-}$ nanosheets, which promote 50 effective electron transfer. Thus, the sheet-like structure of $Cs_4W_{11}O_{36}{}^{2-}$ has suitable properties for constructing a high-performance chromic device.

2 Experimental

2. 1 Synthesis of cesium tungstate ($Cs_4W_{11}O_{36}{}^{2-}$) nanosheets

55 Layered $Cs_4W_{11}O_{36}{}^{2-}$ nanosheets were exfoliated from bulk $Cs_6W_{11}O_{36}$ by a chemical treatment, referring to the previous report.[12] Powder forms of Cs_2CO_3 and WO_3 were mixed at a molar ratio of 3:11 and then ground to a fine powder with a mortar and pestle. The mixed powder was calcined at 1173 K for 60 6 h. After annealing, the resulting dark blue solid ($Cs_6W_{11}O_{36}$) was ground into powder and 0.500 g of the powder was suspended in 50 ml of a 12 M hydrogen chloride (HCl) solution. After stirring the solution for 24 h at room temperature, the solution was centrifuged at 3000 rpm for 10 min and the acidic 65 supernatant was discarded. Fifty milliliters of a 12 M HCl solution was then added and the suspension was again stirred for 24 h. The solution was centrifuged at 3000 rpm for 10 min and the formed yellow precipitate (protonated cesium tungstate; $H_2Cs_4W_{11}O_{36}$) was washed six times with pure water. The 70 precipitate was dispersed in 50 mL of an aqueous tetra(n-butyl)ammonium hydroxide (TBAOH; Aldrich Ltd.) solution to achieve neutral conditions. This suspension was shaken for 10 days at room temperature and yielded a colloidal suspension with a milky appearance. For comparison, commercial WO_3 colloidal 75 solution (Sekisui-Jushi Ltd.) was used in the present study as a conventional chromic material.

2. 2 Thin film fabrication of $Cs_4W_{11}O_{36}{}^{2-}$ nanosheets on aluminum substrate

Aluminum (Al) substrate (1 cm × 1 cm × 1 mm) was washed

by ultrasonication in ethanol for 10 min and surface contaminants were removed by UV-ozone treatment for 30 min. A colloidal suspension of $Cs_4W_{11}O_{36}^{2-}$ nanosheets was coated on the Al substrate using a dipping method. The samples were then dried in
[5] air at room temperature. For comparison, we prepared WO_3 particle-coated Al substrate by a spin-coating of commercial WO_3 colloidal solution.[10]

2. 3 Measurement and analysis

Transmission electron microscopy (TEM; model JEM-2010,
[10] JEOL Instruments, Japan) was used to observe the structure of $Cs_4W_{11}O_{36}^{2-}$ nanosheets using an acceleration voltage of 200 kV. X-ray photoelectron spectroscopy (XPS; model ESCA-5500MT, Perkin Elmer Instruments, Japan) analysis was conducted to determine the chemical states of cesium tungstate using standard
[15] Mg Kα X-rays. Cross-sectional images of the thin films were observed using scanning electron microscopy (SEM; model S-4500, Hitachi Co., Tokyo Japan). Surface morphologies of the mono-layered nanosheet film on the mica substrate were observed by atomic force microscopy (AFM; model SPM-9700,
[20] Shimadzu Instruments, Japan). AFM measurements were performed in the tapping mode under ambient conditions. Absorption spectra for the $Cs_4W_{11}O_{36}^{2-}$/Al and WO_3/Al samples were measured using a spectrophotometer (UV−vis, model V-660, Jasco Instruments, Japan) by a diffuse-reflectance method with
[25] $BaSO_4$ as background. Powder X-ray diffraction (XRD) patterns were recorded with a diffractometer (model SmartLab, Rigaku Instruments, Japan) using Cu Kα radiation (λ=0.15405 nm). Further, XRD patterns of the thin films were measured using out-of-plane and in-plane methods. Coloration was evaluated after
[30] dipping the films in an aqueous HCl solution (pH 2.0) for 5 min using a spectrophotometer as described above.

3 Results and discussion

Layered $Cs_4W_{11}O_{36}^{2-}$ nanosheets were exfoliated from bulk $Cs_6W_{11}O_{36}$ by a chemical treatment, according to the previous
[35] paper.[12] In the present study, we optimized the ratio of the Cs_2CO_3 and WO_3 starting materials to achieve a high production yield of $Cs_6W_{11}O_{36}$ crystal structure. Fig. 1 (a) shows the XRD pattern for the calcined powder when the molar ratio of Cs/W in the starting materials was 4/11, which is the same condition with
[40] the previous report.[12] However, all XRD peaks were assigned to CsW_2O_6, which were not layered structure but formed a three-dimensional tunnel structure. In the present study, the ratio of the starting materials was optimized as Cs/W= 3/11 to achieve a high production yield of the layered $Cs_6W_{11}O_{36}$ structure. The XRD
[45] pattern of $Cs_6W_{11}O_{36}$ synthesized in the present work is shown in Fig. 1 (b). Fig. 1 (c) shows the XRD pattern of protonated cesium tungstate ($H_2Cs_4W_{11}O_{36}$).

Fig. 2 (a) shows photographs for aggregates of bulk $Cs_6W_{11}O_{36}$ and protonated $H_2Cs_4W_{11}O_{36}$ resuspended in a water, and
[50] $Cs_4W_{11}O_{36}^{2-}$ nanosheets in water (pH 7). As $Cs_4W_{11}O_{36}^{2-}$ nanosheets have an anionic surface they are highly dispersed in water even under neutral conditions. TEM analysis revealed that bulk $Cs_4W_{11}O_{36}^{2-}$ was efficiently exfoliated and formed a sheet-like structure in water. The line profile obtained from an atomic
[55] force microscope (AFM) image indicated that the thickness of the $Cs_4W_{11}O_{36}^{2-}$ nanosheet was about 2.3 nm (Fig. 2 (c)), which is

consistent with the reported thickness of a monolayer of a $Cs_4W_{11}O_{36}^{2-}$ nanosheet.[12] A colloidal suspension of $Cs_4W_{11}O_{36}^{2-}$ nanosheets was coated on an Al substrate using a dipping
[60] method. A cross-sectional scanning electron microscopy (SEM) image of the coated Al substrate is shown in Fig. 2 (d). The thickness of the $Cs_4W_{11}O_{36}^{2-}$ nanosheet layer could be controlled by adjusting the concentration of the colloidal suspension and the dipping duration. The thickness of $Cs_4W_{11}O_{36}^{2-}$ nanosheet films
[65] was adjusted to ~500 nm by considering the depth of space charge layer as discussed later.
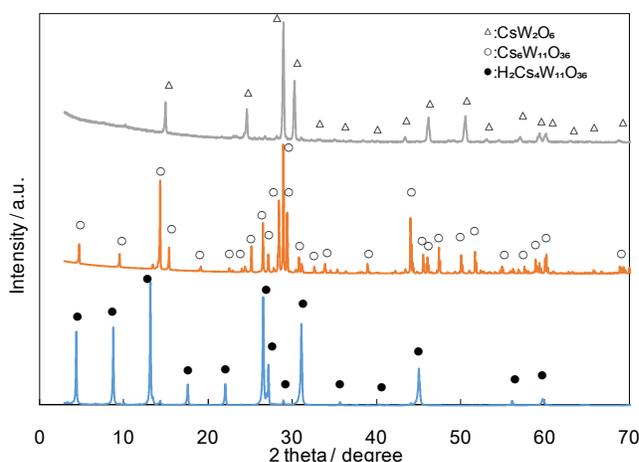
Fig. 1 XRD patterns for powder forms of: (a) bulk CsW_2O_6, (b) layered $Cs_6W_{11}O_{36}$, and (c) protonated layered $H_2Cs_4W_{11}O_{36}$.
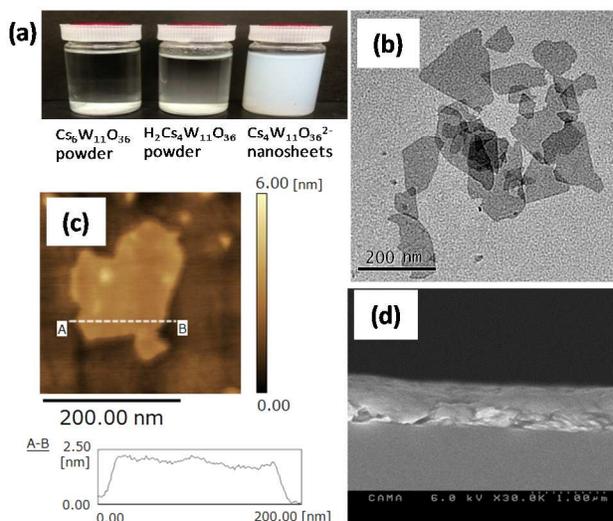
[70] **Fig. 2** Photographs of colloidal solutions of $Cs_6W_{11}O_{36}$ and $H_2Cs_4W_{11}O_{36}$ powders, and $Cs_4W_{11}O_{36}^{2-}$ nanosheets (a). TEM (b) and AFM (c) images of $Cs_4W_{11}O_{36}^{2-}$ nanosheets. The AFM line profile of the $Cs_4W_{11}O_{36}^{2-}$ nanosheet is shown below the AFM image. Cross-sectional SEM image of a thin film of $Cs_4W_{11}O_{36}^{2-}$ nanosheets (d)

[75] In-plane and out-of-plane X-ray diffraction (XRD) patterns of the $Cs_4W_{11}O_{36}^{2-}$ nanosheet films are shown in Fig. 3. Peaks observed in the out-of-plane pattern were assigned to the c-axis of the exfoliated $Cs_4W_{11}O_{36}^{2-}$ plane, while peaks detected in the in-plane pattern were perpendicular to the c-axis. These results

indicate that the exfoliated c-plane of $Cs_4W_{11}O_{36}^{2-}$ nanosheets are attached to the substrate and that the thin film is highly oriented in the direction of the c-axis, which is perpendicular to the Al substrate.
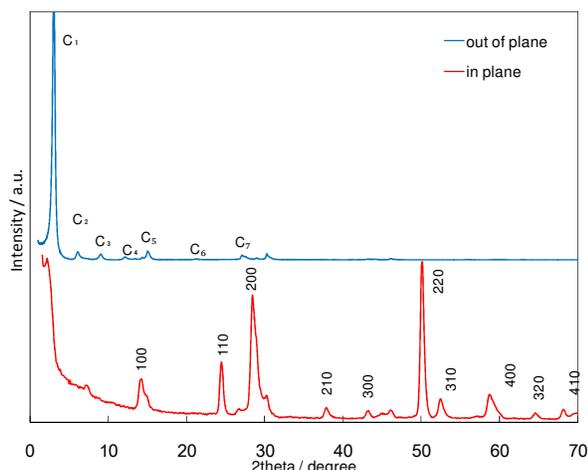
5 **Fig. 3** XRD patterns for a thin film of $Cs_4W_{11}O_{36}^{2-}$ nanosheets. Out-of-plane and in-plane XRD measurements are shown.

Structural analysis on the commercial WO_3 particles as a comparison sample has been conducted and shown in Fig. 4. The thickness of the commercial WO_3 film was similar to that of the 10 $Cs_4W_{11}O_{36}^{2-}$ nanosheet film (about 500 nm).The XRD pattern of the commercial WO_3 revealed that its crystal phase displayed a monoclinic WO_3 structure, and that of the WO_3 film was polycrystalline without any crystal orientation.
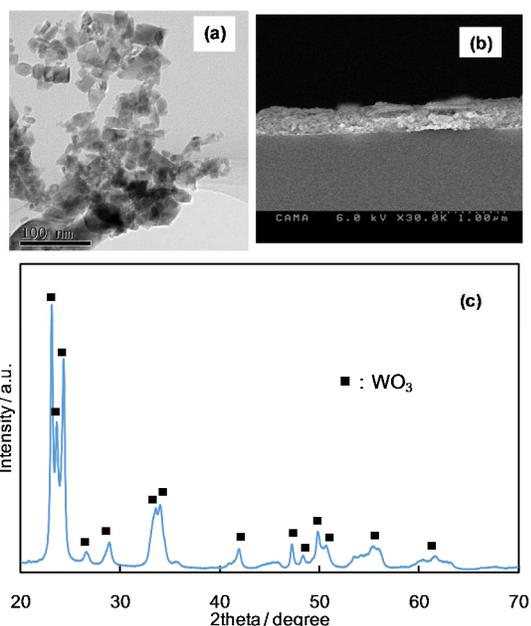
15 **Fig. 4** TEM image of commercial WO_3 particles (a), cross-sectional SEM image of the commercial WO_3-coated thin film (b), and out-of-plane XRD pattern of the thin film of commercial WO_3 (c).

Fig. 5 (a) shows UV-vis absorption spectra recorded by a 20 diffuse reflectance method for the WO_3 and $Cs_4W_{11}O_{36}^{2-}$ thin

films. Before being immersed in aqueous solution, the WO_3 thin film exhibited optical absorption below 460 under atmospheric conditions, a property that is consistent with the band-gap of WO_3. In contrast, the absorption edge of the $Cs_4W_{11}O_{36}^{2-}$ film 25 was observed around 350 nm. These results demonstrate that $Cs_4W_{11}O_{36}^{2-}$ nanosheets have a wider band gap than that of WO_3 particles, owing to the quantum confinement effect of the nanosheet structure. For this reason, the $Cs_4W_{11}O_{36}^{2-}$ nanosheet film appeared transparent, whereas the film of WO_3 particles was 30 yellow. However, after dipping the $Cs_4W_{11}O_{36}^{2-}$ nanosheet and WO_3 films in an aqueous acid solution with the pH value of 2.0 for 2 min, both films turned blue. This coloration effect was induced by the injection of electrons from the Al substrate to the $Cs_4W_{11}O_{36}^{2-}$ nanosheets or WO_3 particles, leading to the 35 reduction of W^{6+} to W^{5+}. Simultaneously with the reduction reaction, protons are injected into the $Cs_4W_{11}O_{36}^{2-}$ and WO_3 crystals.[13, 14] Under these conditions, a broad absorption peak around 650 nm was observed for the WO_3 film, whereas the $Cs_4W_{11}O_{36}^{2-}$ nanosheet film absorbed more photons near infrared 40 region around 800 nm rather than the WO_3 film (Fig. 5 (a)). These results indicate that the potential energy of trapped electrons in $Cs_4W_{11}O_{36}^{2-}$ nanosheets is lower than that of the electrons in WO_3 films. We also evaluated the absorption spectra of thin films by a reflectance mode without using integration 45 sphere unit and can see the obvious color change even under a reflectance mode (see our supporting information, Fig. S1).
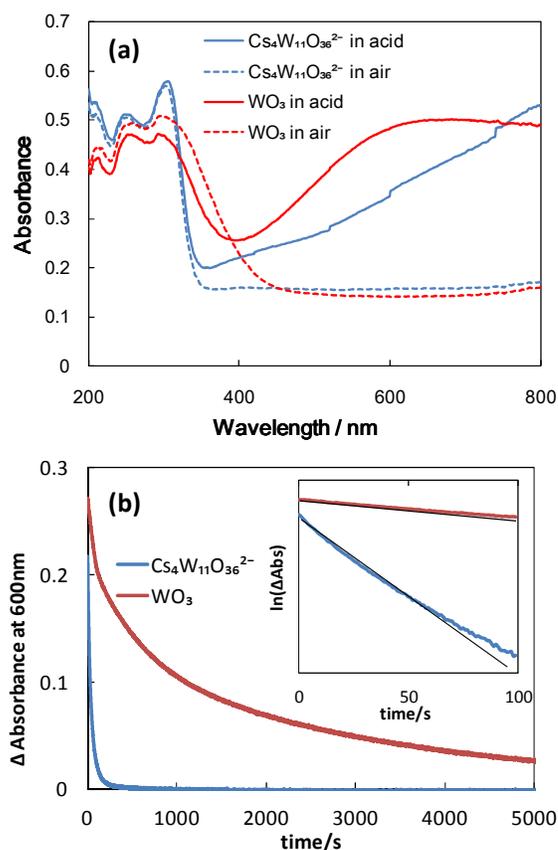
Fig. 5 UV-vis spectra for thin films before and after acid treatment (a). Decay in color (at 600 nm) for thin films in air (b). Inset of (b) shows the relationship between natural logarithm and time.

After exposure to air, the blue substrates returned to their initial color, because the trapped electrons in W^{5+} species reduce oxygen molecules in air. Fig. 5 (b) shows the changes in the
5 absorbance value at 600 nm for the decoloration process under air exposure. Notably, the rate of decoloration of the $Cs_4W_{11}O_{36}^{2-}$ nanosheet film is markedly faster than that of WO_3 film. A plot of the relationship between the natural logarithm of absorbance versus time shows that the decay follows a linear trajectory (Fig.
10 5(b), inset). These results indicate that the decoloration process follows first-order kinetics, a finding that is consistent with the photochromic decoloration process in WO_3.[15] The half-life for the decoloration of $Cs_4W_{11}O_{36}^{2-}$ nanosheets was 25 sec, which was 25-fold more efficient than that of WO_3 particles (650 sec).
15 The Al substrate can be generally oxidized under anodic polarization by an electric field more positive than its redox potential (+1.662 V vs. NHE). In contrast, $Cs_4W_{11}O_{36}^{2-}$ and WO_3 are reduced under cathodic polarization at a potential more negative than their flat-band potentials. When a thin film of a
20 metal oxide semiconductor is coated on an Al substrate, a galvanic potential is generated between the film and the substrate. As the galvanic potential is the driving force that initiates the coloration reaction, the thickness of the semiconductor film should be less than that of the space charge layer between the
25 metal substrate and semiconductor film. We investigated the thickness dependence on the coloring phenomena. When the thickness of tungstate nanosheet was more than two micrometers, the color of this film became inhomogeneous and blue spots were observed around pinholes and cracks of thin films (see our
30 Supporting Information, Fig. S2). In contrast, the color was homogeneous, when the thickness was 500 nm. These results indicate that the thickness for homogeneous coloration should be less than several hundred nanometers. The distance of space charge layer has been estimated by using Poisson's equation, and
35 the estimated distance of space charge layer in the present study is about several micrometers by using a reasonable carrier density as 10^{16} /cm^3 for undoped metal oxide. Our $Cs_4W_{11}O_{36}^{2-}$ and WO_3 films were insulative before coloration, thus the thickness of our film should be less than several micrometers for coloration.
40 Further, the thinner film is better for the diffusion of electrons. But when the thickness of cesium tungstate is too thin, visible light absorption in thin film is not so large and coloration is not obvious. Therefore, the thickness of cesium tungstate nanosheet films in the present study has been adjusted to ~500 nm.
45 In the chromic devices synthesized here, $Cs_4W_{11}O_{36}^{2-}$ or WO_3 are reduced in an acid solution to form color centers, particularly W^{5+}, together with the intercalation of protons in the crystal lattice,[16] whereas Al is oxidized to form Al^{3+} ions, which dissolve into the aqueous acid solution. Fig. 6 shows XPS spectra for the
50 W-4f orbital before and after coloration of the thin film of $Cs_4W_{11}O_{36}^{2-}$ nanosheet. The shape of the XPS curve before acid treatment was deconvoluted into two doublets, where the main doublet at 36.0 eV could be assigned to a W-4f$_{7/2}$ orbital and the other doublet at 38.1 eV was due to W-4f$_{5/2}$, corresponding to the
55 W^{6+} oxidation state. As shown in Fig. 6 (b), a second doublet appeared after acid treatment at lower binding energies of 34.2 and 36.3 eV, which were assigned to W-4f$_{7/2}$ and 4f$_{5/2}$, respectively, and corresponded to the W^{5+} oxidation state. These

results revealed the formation of W^{5+} species after dipping the
60 $Cs_4W_{11}O_{36}^{2-}$ nanosheet into aqueous solution. The percentage of W^{5+} after acid treatment was 21.4%.
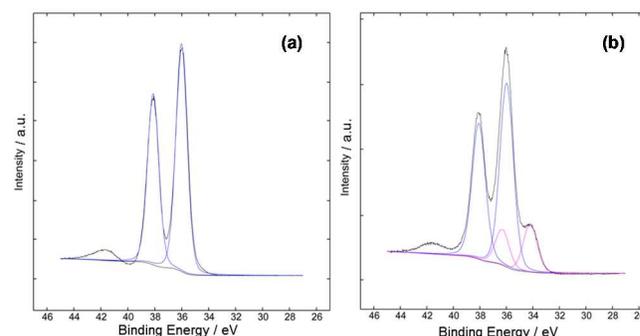
Fig. 6 XPS spectra for the W-4f orbital of $Cs_4W_{11}O_{36}^{2-}$ nanosheet coated on an Al substrate. (a) before acid treatment, (b) after acid treatment.

65

In the decoloration process, reduced tungsten species are oxidized and return to their initial color upon exposure to oxygen. Specifically, electrons trapped at tungsten ions in the crystal lattice diffuse to the nanosheet surface where they react with
70 oxygen molecules in air, reconverting the color of the tungsten species to their initial states. As shown in Fig. 5 (a), the potential energy of trapped electrons in $Cs_4W_{11}O_{36}^{2-}$ are lower than those of trapped electrons in WO_3, indicating that electrons in $Cs_4W_{11}O_{36}^{2-}$ have higher reduction potential. Furthermore, the
75 required diffusion length for trapped electrons in $Cs_4W_{11}O_{36}^{2-}$ is much shorter than that of WO_3 particles, as the thickness of $Cs_4W_{11}O_{36}^{2-}$ nanosheets (2.3 nm) is markedly smaller than the diameter of WO_3 particles (several tens of nm). Thus, the high coloration efficiency observed for $Cs_4W_{11}O_{36}^{2-}$ nanosheets is due
80 to the efficient electron transfer within the sheet-like nanostructure of this material. The plausible scheme for the reversible color change is shown in Fig. 7.
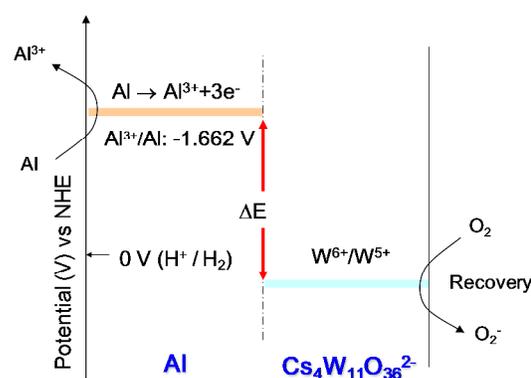
Fig. 7 The plausible scheme for the reversible color change of a thin film
85 of $Cs_4W_{11}O_{36}^{2-}$

The repeatability of coloration and decoloration processes is important for practical applications. Fig. 8 shows the repeatability of the reversible color change in the $Cs_4W_{11}O_{36}^{2}$/Al film upon alternating exposure to acid and ambient air. We confirmed that

coloration and decoloration could be repeated more than 50 times. During the coloration process, the Al substrate was gradually dissolved, however, this dissolution of Al is expected to cease after the full capacity of the $Cs_4W_{11}O_{36}^{2-}$ nanosheet for

5 electrons is reached. In the present study, the $Cs_4W_{11}O_{36}^{2-}$ nanosheet layer had a thickness of only 2.3 nm, making its capacity for electrons very small. Here, we speculate on the reasonable life time of our device based on the electrochemical point of view. We assume a reasonable carrier density in a bulk

10 as small polarons from 10^{18} to 10^{20}/ cm^3 in tungsten oxide compounds.[17,18] Under these consideration, one coloration/decoloration cycle consumes Al substrate, which corresponds to the Al thickness from 0.0027 nm to 0.27 nm. Therefore, the long term durability can be expected in our

15 chromic device, and our chromic device is very robust under repeated coloration and decoloration process.
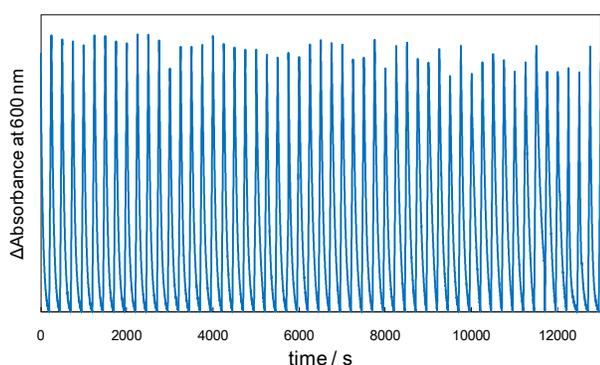
Fig. 8 Repeatability of the reversible color change in $Cs_4W_{11}O_{36}^{2-}$ nanosheets/Al by acid treatment and exposure to air at room temperature.

20

In addition to rapid coloration, our $Cs_4W_{11}O_{36}^{2-}$ nanosheet is superior to conventional WO_3 particles because of its colorlessness in visible light range before dipping in aqueous solution. Further, our $Cs_4W_{11}O_{36}^{2-}$ nanosheet is very stable in

25 alkaline condition, whereas conventional WO_3 particles are dissolved in alkaline solution. Figure 9 shows the photos before and after dipping in aqueous solution. Our $Cs_4W_{11}O_{36}^{2-}$ nanosheet exhibited reversible coloration even in an alkaline condition. And our $Cs_4W_{11}O_{36}^{2-}$ nanosheet is very stable in alkaline condition,

30 while conventional WO_3 particles are dissolved in alkaline solution.
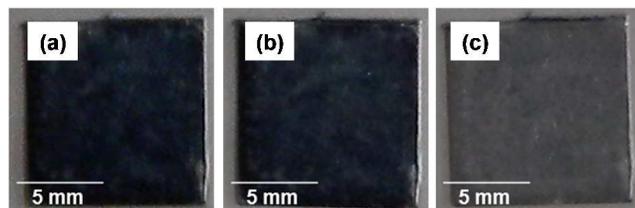
Fig. 9 Photos of $Cs_4W_{11}O_{36}^{2-}$ nanosheet films after dipping in acid with pH= 3(a), in alkaline solution with pH= 11 (b), and before coloration (c).

35 **4 Conclusions**

We have developed a novel, reversible chromic device consisting of a $Cs_4W_{11}O_{36}^{2-}$ nanosheet film on an Al substrate, for

which an aqueous acid solution and oxygen exposure act as the ink and eraser, respectively. The efficient coloration of this

40 material is due to its sheet-like nanostructure. Our chromic device is comprised of non-toxic inorganic materials that are robust under heat treatment and does not require light or electric power sources, complicated sandwich cell structure, or a transparent electroconductive substrate, such as ITO or FTO glass. Hence,

45 the chromic device described here is potentially suitable for various industrial and commercial applications, including displays, data storage devices, and sensors.

Notes and references

a Graduate School of Science and Engineering, Tokyo Institute of Technology, 2-12-1 Ookayama, Meguro-ku, Tokyo 152-8552 Japan

60 *Fax: ;81 3 5734 3368; Tel: 81 3 5734 2527; E-mail: mmiyauchi@ceram.titech.ac.jp*

b PRESTO, JST, 4-1-8 Honcho Kawaguchi, Saitama 332-0012 Japan

† Electronic Supplementary Information (ESI) available: TEM and XRD analysis on the conventional WO_3 powder and thin film, UV-Vis spectra

65 measured by reflection mode, Photos of films under alkalline condition. See DOI: 10.1039/b000000x/

1   S. K. Deb and J. L. Forrestal, in *Photochromism* (Eds: G. H. Brown), Wiley-VCH, New York, 1971, 633.

70 2   C. G. Granqvist, *Handbook of Inorganic Electrochromic Materials*, Elsevier, Amsterdam, 1995.

3   R. J. Colton, A. M. Guzman and J. W. Rabalais, *Acc. Chem. Res.,* 1978, **11**, 170.

4   B. W. Faughnan and R. S. Crandall, *Topics in Applied Physics,* 1980,

75   **40**, 181.

5   C. S. Blackman and I. P. Parkin, *Chem. Mater.,* 2005, **17**, 1583.

6   C. Bechinger, E. Wirth and P. Lederer, *Appl. Phys. Lett.,* 1996, **68**, 2834.

7   C. M. Lampert, *Solar Ener. Mater.,* 1984, **11**, 1.

80 8   P. Delichere, P. Falaras, M. Froment, H. L. Goff and B. Agius, *Thin Solid Films,* 1988, **161**, 35.

9   Z. G. Zhao, Z. F. Liu and M. Miyauchi, *Adv. Funct. Mater.,* 2010, **20**, 4162.

10   M. Miyauchi, Y. Li, S. Yanai and K. Yotsugi, *Chem. Commun.,*

85   2011, **47**, 8596.

11   M. S. Paley, E. J. Meehan, C. D. Smith, F. E. Rosenberger, S. C. Howard and J. M. Harris, *J. Org. Chem.,* 1989, **54**, 3432.

12   K. Fukuda, K. Akatsuka, Y. Ebina, R. Ma., K. Takada, I. Nakai and T. Sasaki, *ACS Nano,* 2008, **2**, 1689.

90 13   Z. Liu, Z. Zhao and M. Miyauchi, *J. Phys. Chem. C* 2009, **113**, 17132.

14   Q. Zhong, K. Colbow, *Thin Solid Films,* 1991, **205**, 85.

15   E. Kikuchi, N. Hirota, A. Fujishima, K. Itoh and M. Murabayashi, *J. Electroanal. Chem.,* 1995, **381**, 15.

95 16   J. Hou, G. Zuo, G. Shen, H. Guo, H. Liu, P. Chen, J. Zhang and S. Guo, *Nanoscale Res. Lett.,* 2009, **4**, 1241.

17   E. Salje, *J. Appl. Cryst.* 1974, **7**, 615.

18   J. Ederth, A. Hogel, G. A. Niklasson and C. G. Granqvist, *J. Appl. Phys.* 2004, **96**, 5722.

100

Tungstate nanosheet ink as a photonless and electroless chromic device

Masahiro Miyauchi,* Akihiko Kondo, Daiki Atarashi, Etsuo Sakai
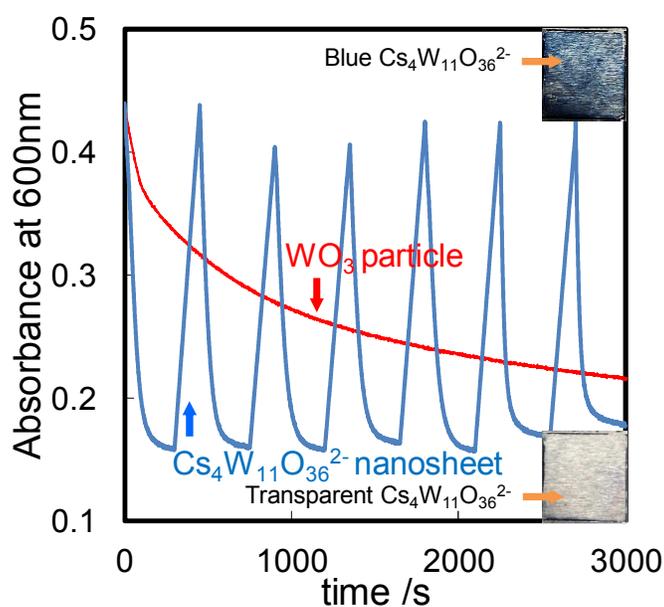
Cesium tungstate ($Cs_4W_{11}O_{36}^{2-}$) nanosheets exhibits an efficient reversible color change without light irradiation or an electric power supply.